frontiers | Frontiers in Earth Science

TYPE Original Research
PUBLISHED 11 July 2024
DOI 10.3389/feart.2024.1410011

OPEN ACCESS

EDITED BY
Emanuele Intrieri,
University of Florence, Italy

REVIEWED BY
Pengju An,
Ningbo University, China
Zhilu Chang,
Nanchang University, China

*CORRESPONDENCE
Demin Xue,
284636713@qq.com
Shuai Zhang,
zhangshuaiqj@zju.edu.cn

RECEIVED 31 March 2024
ACCEPTED 21 June 2024
PUBLISHED 11 July 2024

CITATION
Wu Y, Xue D, Chen K, Dai C, Hang Z, Wu Z and Zhang S (2024), Failure mechanism and early warning of an excavation-induced soil landslide.
Front. Earth Sci. 12:1410011.
doi: 10.3389/feart.2024.1410011

Failure mechanism and early warning of an excavation-induced soil landslide

Yingfeng Wu[1], Demin Xue[1,2,3]*, Kai Chen[1], Cong Dai[4], Zhenyuan Hang[1], Zhongteng Wu[2,3] and Shuai Zhang[4,5]*

[1]Zhejiang Institute of Communications, Hangzhou, Zhejiang, China, [2]Key Laboratory of Geohazard Prevention of Hilly Mountains, Ministry of Natural Resources, Fuzhou, China, [3]Fujian Key Laboratory of Geohazard Prevention, Fuzhou, China, [4]MOE Key Laboratory of Soft Soils and Geoenvironmental Engineering, Institute of Civil Engineering, Zhejiang University, Hangzhou, Zhejiang, China, [5]State Key Laboratory of Geohazard Prevention and Geoenvironment Protection, Chengdu University of Technology, Chengdu, China

Due to the uncertainty in soil landslide failure mechanisms, lack of early warning systems for soil landslides and adoption of improper excavation configurations, soil landslides accidents triggered by highway excavation in Chinese mountainous areas generally require expensive remedial measures. This paper describes a soil landslide associated with excavation through integrating field reconnaissance and finite element method simulation. According to the obtained results, the adoption of toe excavation and the presence of a silty clay layer are the two main factors contributing to the failure of the soil landslide, and a strong negative correction was observed between the toe excavation and surface displacement and the safety factor of the investigated cut slope; therefore, a four-level early warning system for this excavation-induced soil landslide was established by employing toe excavation and surface displacement thresholds as the warning indicators. Lastly, a preferable excavation configuration was proposed to facilitate excavation designs in similar landslide-prone areas.

KEYWORDS

landslide, excavation, mechanism, early warning, finite element method

1 Introduction

Cut slopes have been extensively developed during highway construction in mountainous areas, some of which failed due to improper excavation accidently, accounting for half of all casualties related to highway construction in mountainous areas (Hiraoka et al., 2017) and resulting in considerable additional investment and time for implementing measures to prevent such excavation-induced landslides (Li et al., 2011; Zhang et al., 2015; Lin et al., 2017; Khanna and Dubey, 2020; Gao et al., 2022). The stability and failure mechanisms of cut slopes under toe excavation unloading conditions are critical issues that have been researched by many scholars. Among the three important highway cut slopes developed in the Uttarakhand Himalayan terrain, the most unstable cut slope had a safety factor less than unity according to finite element method (FEM) modelling (Pradhan et al., 2018). Ten road cut slopes developed during excavation in the Kullu area of India were characterized as having a low stability (Khanna and Dubey, 2020). The critical excavation depth for two idealized jointed rock slopes was investigated using a face-to-face discrete element method (Li et al., 2007). The influence of the excavation

unloading path and rate on the slope stability was analysed in detail (Li et al., 2014; Won, et al., 2014; Wang et al., 2020). The influence of slope shape on the stability of soil slopes has been studied, revealing that slope stability is negatively correlated with the slope ratio under constant slope height conditions (Wu and Wang, 2020). The excavation dynamic load-increasing displacement response ratio, obtained by using the FEM strength reduction method, was proposed to evaluate the stability of an ancient landslide during toe excavation (Wu et al., 2022). The failure mechanisms associated with cut slopes, including progressive failure (Zhang et al., 2014; Mohammadi and Taiebat, 2016; Zhao and Zhang, 2018), translational failure (Stark et al., 2005; Xue et al., 2018; Zhu et al., 2021), toppling failure (Zhu et al., 2020), and arching failure (Fang et al., 2022; Fang et al., 2023) have been explained via indoor modelling tests and numerical simulations. However, exploring the failure mechanisms of highly susceptible cut slopes during excavation is still necessary due to complex slope materials, complex geological conditions, variations in climate, etc.

Early warning for landslides is highly important (Medina-Cetina and Nadim, 2008; Thiebes et al., 2014; Manconi and Giordan, 2015; Liu et al., 2024; Zhang et al., 2024), and early warning systems have been designed for specific sites (Intrieri et al., 2012; Michoud et al., 2013; Dikshit et al., 2019), with critical warning parameters that vary depending on the type of landslide and failure mechanism (Lacasse and Nadim, 2009; Manconi and Giordan, 2015). For instance, the empirical waning model for predicting the failure of rainfall-induced landslide mainly depends on the functional relationship between rainfall measurement and landslide events (Mirus et al., 2018; Chen et al., 2019). A site-specific landslide early warning model for predicting the progressive slope instability is focused on deformation rate, rate increment and tangential angle of surface displacement (Ju et al., 2020). What's more, the initial deformation pattern of the landslide was utilized as a predictor for the final global failure (Dick et al., 2015; Intrieri et al., 2018). The multiple warning levels are essential components of the warning model (Pecoraro et al., 2019; Guzzetti et al., 2020). However, due to individual differences in the characteristics and failure mechanisms of different slopes, the design of warning models, including thresholds with warning levels, remains a complex issue, and there is no uniform design standard worldwide (Pecoraro et al., 2019). For excavation-induced landslides, the relationship between the amount of excavation associated with slope behaviours can be accurately established using numerical simulations incorporating detailed field reconnaissance (Xue et al., 2018; Wu et al., 2022); therefore, an early warning system should be established accordingly. However, there are a few studies on the early warning system of soil slopes under roadway excavation.

FIGURE 1
Location of the study area.

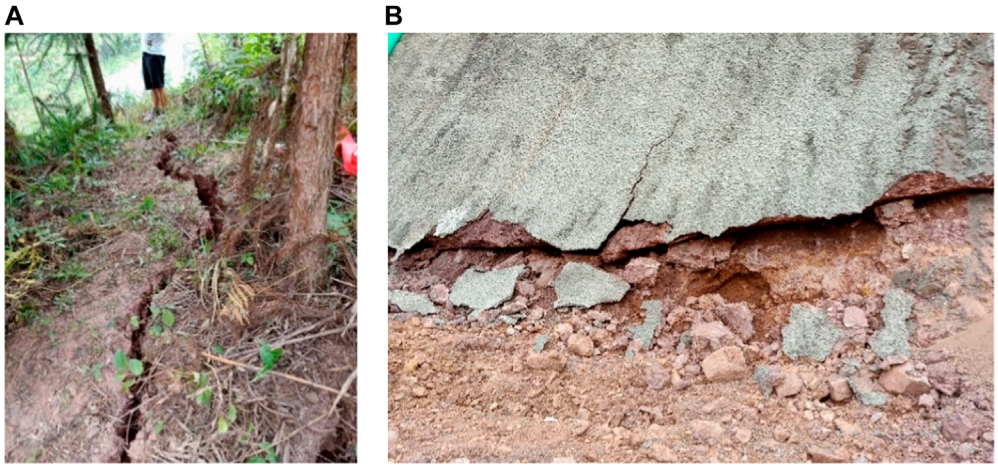

FIGURE 2
Evidence of deformation of cut slope. **(A)**: A tension crack in the crown, **(B)**: A shearing outlet at the toe.

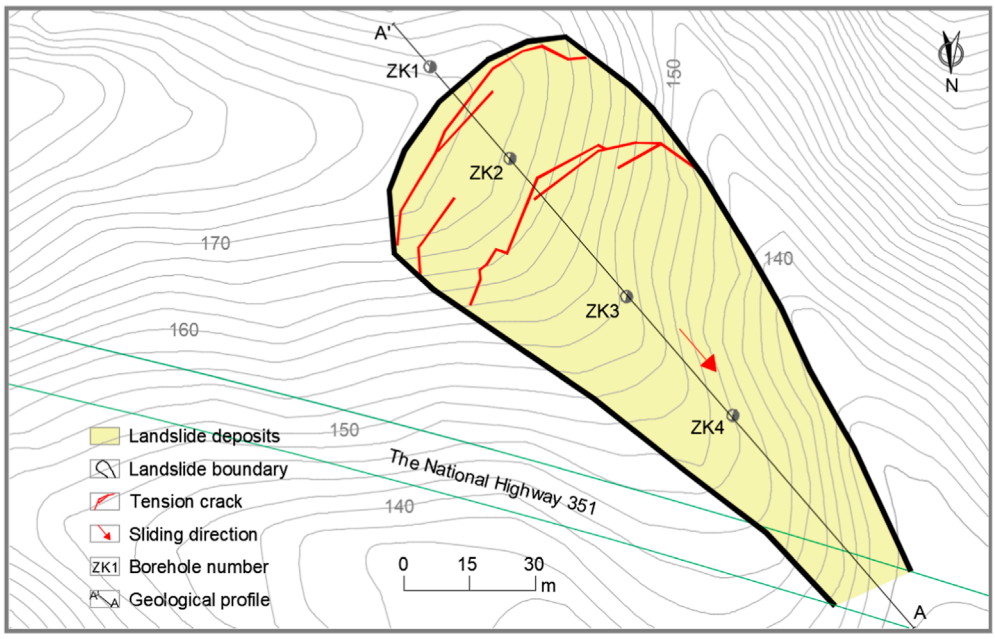

FIGURE 3
Geological map of the soil landslide.

This paper focuses on a soil landslide case involving toe excavation, which poses a considerable threat to the safety of the construction of National Highway 351. The aim of this study is to provide key information for the mitigation of future landslides via an analysis of the possible evolution and mechanisms of slope failure. Field reconnaissance, including geological surveys, drilling surveys and *in situ* deformation monitoring and laboratory tests of slope materials extracted from boreholes were carried out. A series of FEM analyses considering different excavation configurations was also completed. With the field reconnaissance and FEM simulation results, the influence of excavation on slope stability was evaluated, and the failure mechanism of the soil landslide was explored. Furthermore, an early warning system was preliminarily proposed for reducing the risk of landslides. Finally, a reasonable excavation configuration was discussed to provide a reference for the treatment of similar soil landslides.

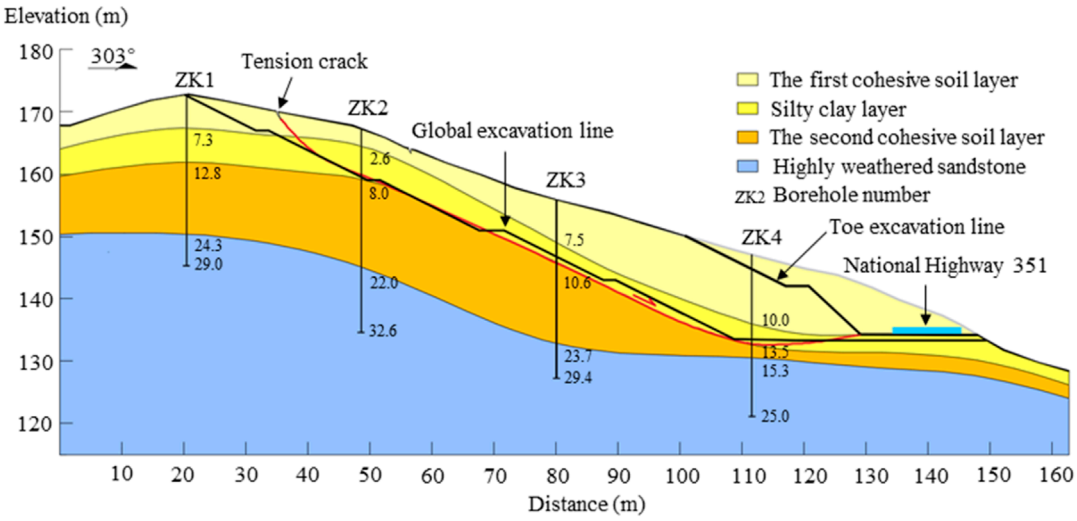

FIGURE 4
Geological profile AA′ of the excavated slope. Its location is shown in Figure 3.

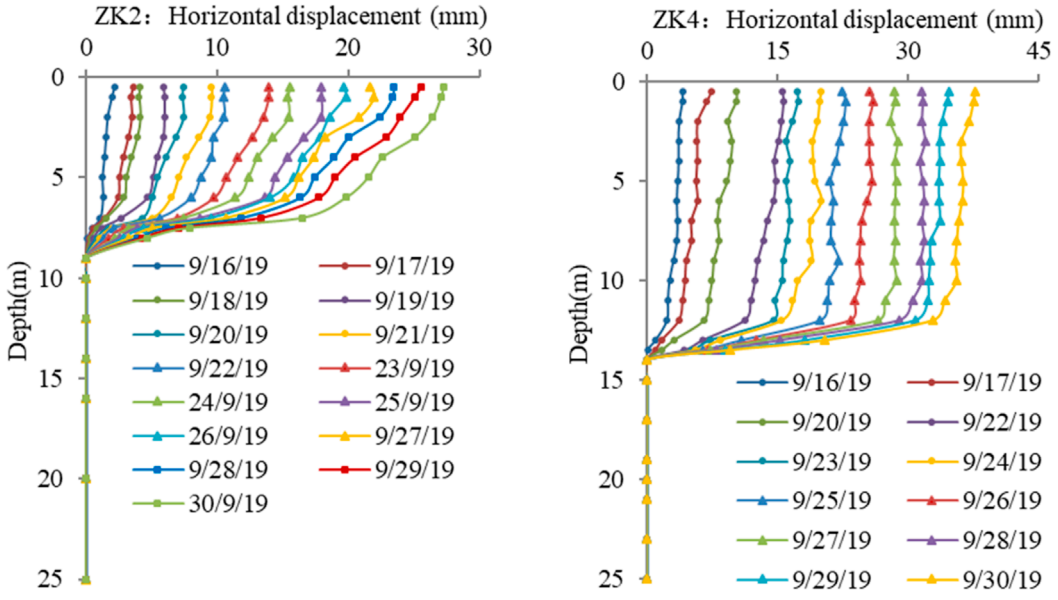

FIGURE 5
Horizontal displacements of the excavated slope before the emergency treatment project.

2 Study area

The study area (Figure 1) is characterized by a mountainous hilly terrain with altitudes ranging between 130 and 350 m and slope angles ranging between 15° and 20°; vegetation coverage is common here. The study area experiences four distinct seasons and abundant rainfall, with 140 annual average rainy days, an average precipitation of 1762.1 mm, and a historical maximum daily precipitation of 289 mm. The rainy season is from April to June, and the dry season in this area is from July to October. During September 2019, the large highway excavation for National Highway 351 was completed, and some evidence of deformation of cut slope was clearly found, including a series of large transverse tension cracks in the slope crown (Figure 2A) and an obvious shearing outlet at the excavated slope toe (Figure 2B). The angle between the sliding direction and highway direction was approximately 35° (Figure 3). The deformation and failure of this excavated slope seriously threatened the safety of highway construction; therefore, special attention should be given to the failure mechanism and corresponding mitigation measures of this cut slope.

TABLE 1 Material properties used in the slope stability analysis.

Parameter	The first cohesive soil layer	Silty clay layer	The second cohesive soil layer	Highly weathered sandstone	Pre-reinforced pile
Unit weight γ (kN/m^3)	19.8	19.4	20	22	
Cohesion c (kPa)	10	9.4	12	30	
Friction angle φ (°)	25	15	28	32	
Elastic modulus E (kPa)	500·10^3	300·10^3	800·10^3	3300·10^3	3·10^8
Poisson's ratio υ	0.25	0.3	0.2	0.2	
Moment of inertia (m^4)					4.5

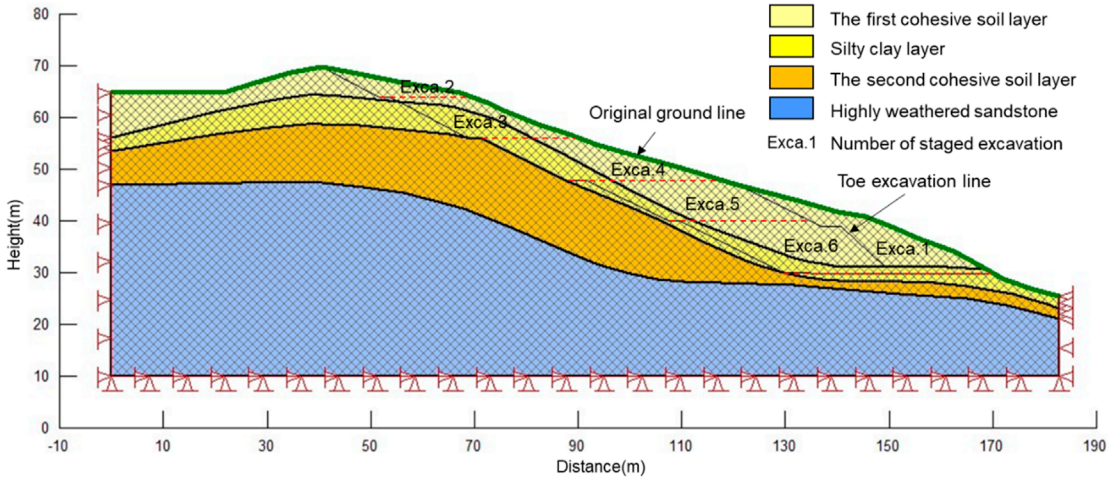

FIGURE 6
2D FEM mesh for the original slope.

3 Investigation methodology

Site investigations, including geological surveys, drilling surveys, and surface and deep displacement monitoring, were rapidly conducted after the occurrence of obvious deformation of the excavated slope. Four boreholes, ZK1, ZK2, ZK3 and ZK4, were drilled in the excavated slope, as shown in Figures 3, 4. According to the drilling data, from the surface downward, the composition of the excavated slope include the following materials: (1) the first cohesive soil layer, mixed with substantial crushed stones with particle diameters of 2–6 cm, greyish–yellow and yellowish–brown, 2.6–10 m thick; (2) the silty clay layer, purplish–red, 3.1–5.5 m thick, easily broken when pinched by hand, indicating that this soil layer has a low strength; (3) the second cohesive soil layer, mixed with massive crushed stones with particle diameters of 4–10 cm, purplish–red and greyish–white, 1.8–13.1 m thick; and (4) highly and moderately weathered fractured sandstone, greyish–yellow and cyan–grey, respectively, with a recorded maximum depth of 32.6 m. No groundwater was found in the four boreholes. According to the results of the geological and drilling surveys, the deformed excavated slope is a soil landslide with a longitudinal length of 110 m, a horizontal width of 50 m, an average thickness of 8.5 m, an area of 4,500 m^2 and a volume of 3.6×10^4 m^3.

Deep displacement monitoring was immediately conducted to evaluate the stability of the excavated slope. Two inclinometers were installed in boreholes ZK2 and ZK4 to detect the deep displacement of the excavated slope and the position of the potential sliding surface. The recorded surface displacements show that the excavated slope continued to deform at a rate of approximately 1.43–3.16 mm per day. The continuously recorded deep displacements for the 15 days before the mitigation project are shown in Figure 5. Notably, the excavated slope experienced progressive deformation; moreover, the magnitude of displacement of the leading edge of the slope was significantly larger than that of the trailing edge, indicating that the deformed excavated slope was a traction-type soil landslide. According to the deep displacement monitoring data, a sliding surface was clearly identified in the silty clay layer at depths of 8 m and 13.5 m in boreholes ZK2 and ZK4, respectively. The identified sliding surface is shown in Figure 4. The above site investigation results show that the excavated slope continuously slid at a relatively

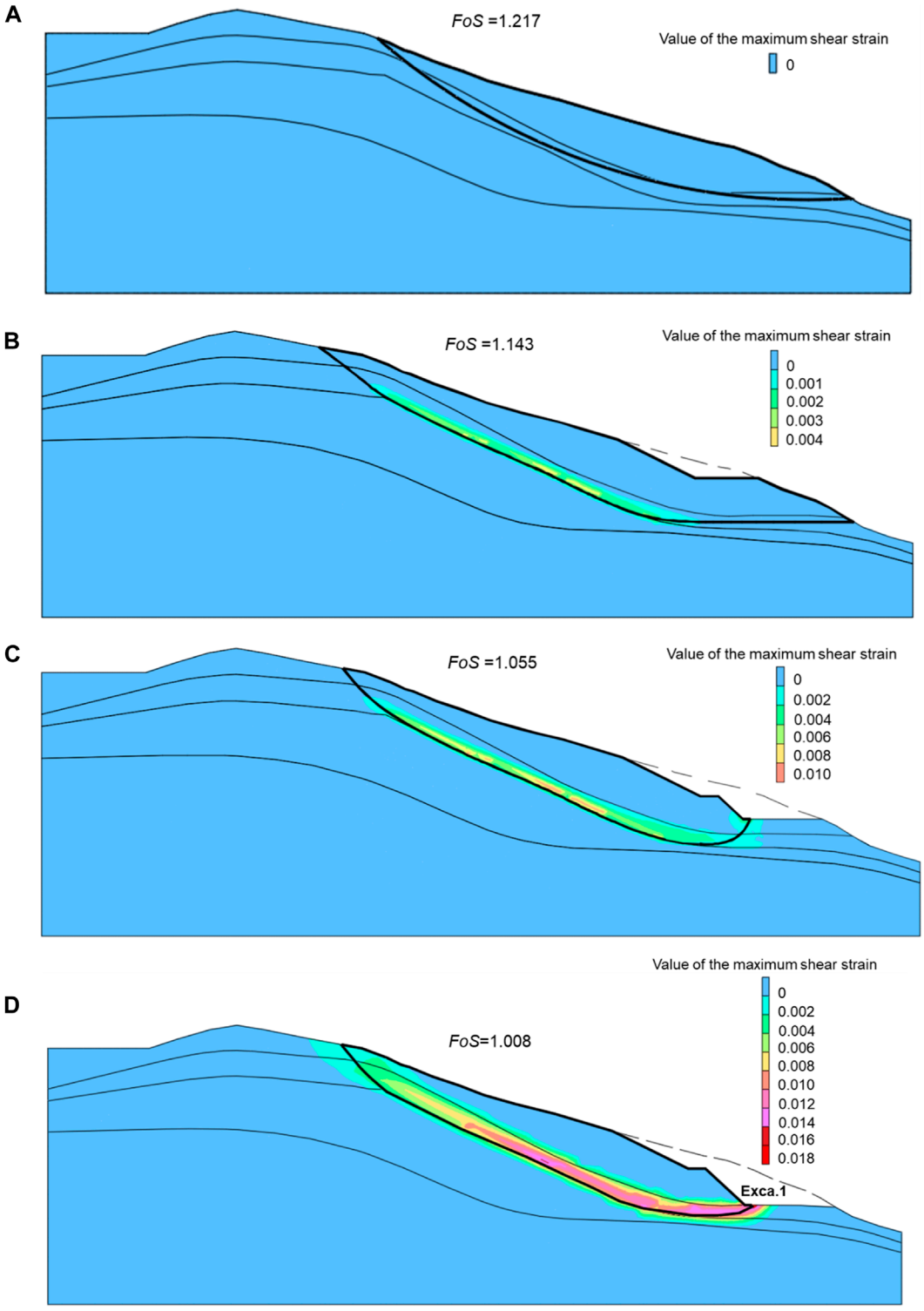

FIGURE 7
The factor of safety *FoS* for the slope before and after the first excavation (i.e., toe excavation which is developed in three steps). **(A)**: No excavation, **(B)**: 1st-step excavation, **(C)**: 2nd-step excavation, **(D)**: 3rd- step excavation.

slow rate along the sliding surface developed in the silty clay layer; thus, necessary measures should be carried out to mitigate further issues.

As revealed by the site investigation, the excavated slope consists of the first cohesive soil layer, the silty clay layer, and the second cohesive soil layer between the ground surface and the

bedrock, and it was progressively deformed along the silty clay layer. Laboratory direct shear tests of undisturbed specimens of silty clay and two kinds of cohesive soils extracted from borehole ZK1 were performed to determine their shear strength parameters by using a ZJ-2 strain-controlled direct shear apparatus. The obtained test results are shown in Table 1. The shear strength parameters of the silty clay layer are much lower than those of the two kinds of cohesive soils. Accordingly, the poor shear strength of the silty clay layer in the excavated slope is unfavourable for slope stability.

4 FEM stability analysis considering excavation

To reproduce the deformation evolution of the studied slope from before to after highway excavation and to evaluate the corresponding slope stability, ultimately, to explore the genetic mechanism of the deformed slope, 2D FEM analysis incorporating stability analysis was conducted by using Sigma-W software and Slope-W software (GEO-SLOPE International Ltd., 2007). In the Sigma-W analysis, the deformation evolution of a slope can be clearly highlighted, and the potential sliding surface can be determined by the maximum shear strain (Li et al., 2013; Xue et al., 2018). In the Slope-W analysis, a FEM stress-based method is used to calculate the factor of safety *FoS* for the slope during the deformation evolution process. Special attention should be given to the silty clay layer in this case study due to its shear strength being lower than that of the surrounding cohesive soil layers, indicating that the sliding surface is more likely to develop along the silty clay layer. Thus, the accuracy of the critical failure surface in Slope-W should be verified by the maximum shear strain in Sigma-W.

The physical and mechanical parameters of the slope materials were determined via laboratory tests and are shown in Table 1. Figure 6 represents the FEM mesh for the original slope. No horizontal displacement boundaries are set along the left and right side boundaries, and no horizontal and no vertical displacement boundaries are set along the bottom boundary of the model. The excavation process is modelled using an unloading element in Sigma-W. The model materials are assumed to comply with the Mohr–Coulomb failure criterion in Sigma-W. The initial stresses of the Sigma-W model are gravity stresses. The simulation starts with the original slope, and subsequent excavations, including toe excavation for highway construction and global excavation for treating the deformed slope, are performed in six steps.

The original slope is in a stable state with a *FoS* of 1.217, which has no shear deformation in the silty clay layer (Figure 7A). However, the slope stability gradually decreases during the three-step excavation process at the toe, the maximum shear deformation initially occurs in the silty clay layer (Figure 7B), and then propagates towards the toe of excavated slope as the toe excavation increases significantly (Figure 7C). After the first excavation (i.e., toe excavation) is completely constructed, the final excavated slope is approximately in a limit equilibrium state with a *FoS* of 1.008, and a well-developed sliding surface occurs ultimately (Figure 7D). The above results indicate that toe excavation significantly reduces

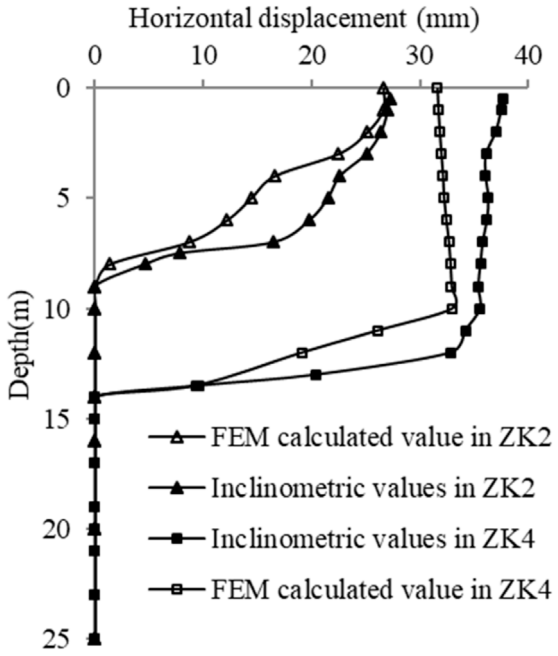

FIGURE 8
The horizontal displacements of the cut slope after toe excavation from FEM simulation and inclinometer measurements.

the slope stability. The initiation and propagation progress of the sliding surface in the excavated slope shows that the weak silty clay layer essentially facilitates the deformation of the slope under toe excavation conditions. The horizontal displacements of the slope after toe excavation were also calculated by FEM software. Two typical horizontal displacement profiles are shown in Figure 8, which shows that the horizontal displacements of the upper excavated slope are obviously smaller than those of the lower slope, indicating traction deformation characteristics. The FEM analysis results are in good accordance with the results of the site investigation, although the FEM-based displacements are slightly less than the inclinometer measurements.

To completely remove the threat of the deformed slope, a global excavation scheme for the deformed cut slope was designed (Figure 4), which included five-stage excavations from the top to the toe of the deformed slope, i.e., Exca. 2, Exca. 3, Exca. 4, Exca. Five and Exca. 6 (Figure 6). A series of FEM slope stability analyses was conducted utilizing the preexisting sliding surface in the deformed slope before Exca. 6, whereas the critical sliding surface identified by Slope-W software was used when the deformed slope was completely dug out after Exca. 6. Figure 9 represents *FoS* for the excavated slope *versus* the ratio of cumulative excavation to the deformed slope. In this figure, the *FoS* for the excavated slope gradually increases from 1.008 to 1.85 with increasing excavation of the deformed slope before Exca. 6, ultimately reaching 1.613 after Exca. 6. The above significant increase in *FoS* confirms that global excavation from the top to the toe of the deformed slope is a remarkably effective emergency mitigation measure, greatly improving the stability of the deformed slope.

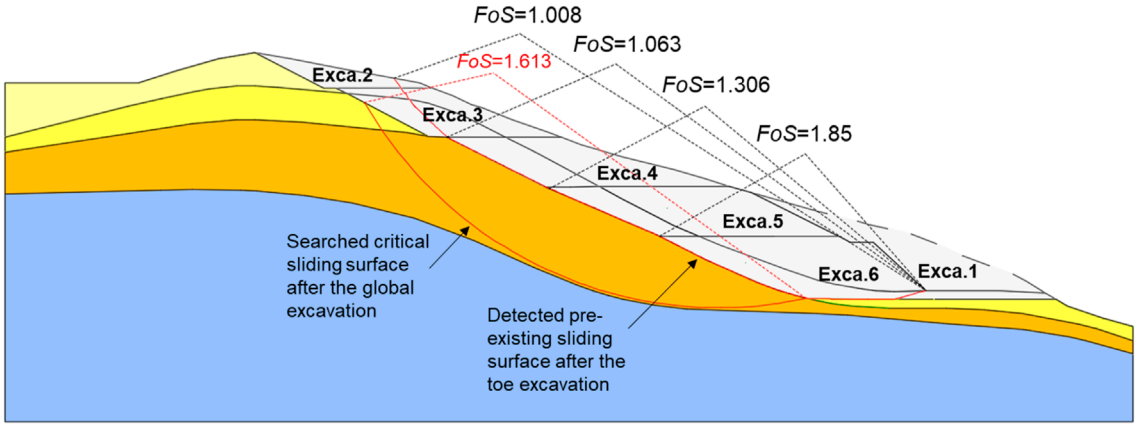

FIGURE 9
The factor of safety *FoS* for the excavated cut slope during global excavation.

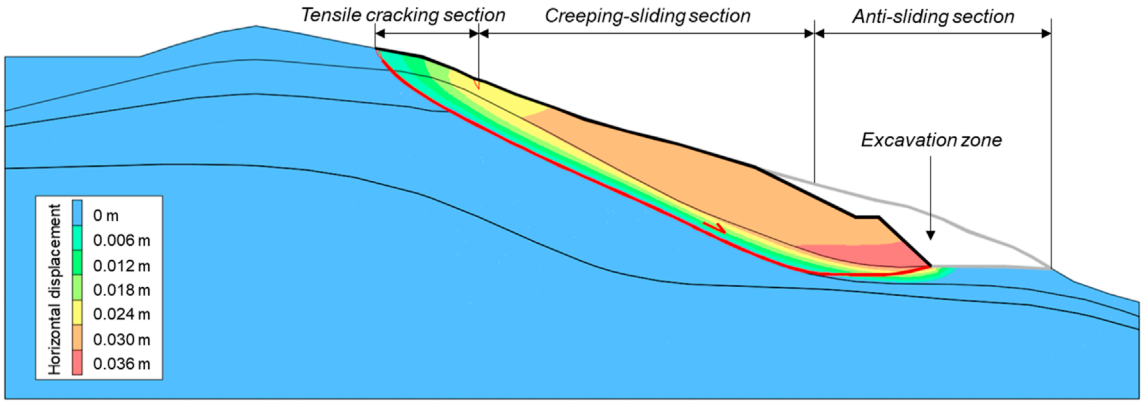

FIGURE 10
The geo-mechanical model of cut slope failure.

5 Failure mechanism of the cut slope

According to the results of the FEM analysis and site investigation, inappropriate toe excavation of the slope, which reveals the weak clay silty layer, creates a larger free surface, and decreases the anti-sliding force, leads to the sliding deformation of the cut slope. Moreover, the weak clay silty layer easily evolves into a sliding surface due to its low shear strength, as revealed by the FEM and inclinometer results, and the cut slope progressively deforms along the weak clay silty layer (see Figure 7). It is reasonable to conclude that the main factors contributing to the deformation of the cut slope are adoption of toe excavation and the presence of a weak silty clay layer. According to the Varnes classification of landslide types (Hungr et al., 2014), a deformed slope is a progressively retrogressive soil landslide. The geo-mechanical model of cut slope failure can be defined as traction creeping-sliding tensile-cracking model, which is shown in Figure 10. Such soil landslides are typically characterized by greater deformation in the lower slope than in the upper slope, as demonstrated by Figures 8, 10, which is conducive to the early warning and prevention of such landslides. For this case study, considering these typical characteristics, global excavation from the top to the toe of a deformed cut slope is an effective emergency mitigation measure for guaranteeing the stability of the final cut slope.

6 Early warning of the cut slope failure

As mentioned above, the deformation of a slope with a weak clay silty layer caused by toe excavation for highway construction was an unpredictable landslide incident, indicating the importance of a landslide early warning system aimed at protecting construction personnel and equipment during the process of toe excavation. Therefore, an early warning system for this kind of landslide is specifically designed by integrating the results of FEM simulations and field monitoring. In this study, the determination of the early warning level is based on the factor of safety of slope *FoS*, which is universally applied to evaluate slope stability. As shown in

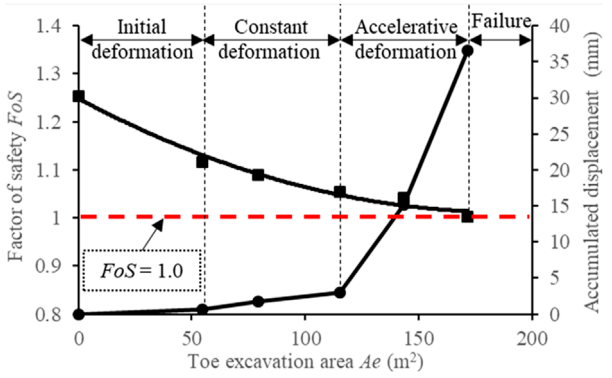

FIGURE 11
FEM results of slope stability and displacement with respect to toe excavation in the case of a cut slope ratio of 1:1; the excavation line is shown in Figure 6.

Figure 7, toe excavation with a cut slope ratio of 1:1 significantly decreases the slope stability; thus, toe excavation is clearly a key factor to consider in early warning efforts. Considering different degrees of toe excavation, many additional FEM simulations were performed. The obtained factor of safety of the slope *FoS* and the horizontal displacement related to toe excavation is shown in Figure 11. A strong negative correlation between the slope stability (*FoS*) and the progress of toe excavation was clearly observed, demonstrating the disadvantageous impact of toe excavation on the slope stability. In addition, the calculated displacement shows a three-stage deformation characteristic to some extent: the initial deformation stage, during which the factor of safety *FoS* is greater than 1.1; the constant deformation stage, during which the factor of safety *FoS* ranges from 1.05 to 1.1; the accelerated deformation stage, during which the factor of safety *FoS* ranges from 1.05 to 1.0; and the failure deformation stage, corresponding to a factor of safety *FoS* less than 1.0. According to the obtained *FoS* threshold for each level of slope stability, the threshold of toe excavation for the corresponding early warning level were computed. For example, when the excavated slope reaches the limit equilibrium state (*FoS* =1.0), the threshold of toe excavation equals 171.43 m^2; once this threshold is exceeded, a landslide occurs. Ultimately, considering the peculiarity and importance of highways, referring to the methods proposed by Xu et al. (2009, 2011, 2016) and Fan et al. (2019), a preliminary early warning system for the excavation-induced landslide of the studied slope with a weak layer was developed based on the above two early warning parameters, as shown in Table 2. Corresponding countermeasures are recommended for each warning level.

The main features of early warning system are the choice of the warning levels. Here four levels were suggested as the optimum solution because more levels would require the identification of more thresholds without considerable improvement and thus cause a meaningless loss of simplicity, compromising the whole system (Intrieri et al., 2012). Furthermore, increasing the number of warning levels can be less cost-effective (Medina-Cetina and Nadim, 2008). The selection of appropriate thresholds is highly important. At present, the toe excavation data, along with the factor of safety *FoS*, were exploited as warning threshold because of the good correlation between the amount of excavation and displacement observed (see Figure 11). According to the acceptable risk criteria (Xu et al., 2011), the above thresholds are straightforwardly defined, incorporate four different levels, and are representative of the landslide behavior. Note that the alarm level can be scarcely reached due to manual treatment measures implemented before imminent landslide failure.

The excavation-induced landslide warning platform design is still in progress, configuring the web-based visualization of site-specific landslide monitoring system, FEM slope stability calculations corresponding to actual toe excavation, and the web notification service which automatically sends mobile SMS and email messages to subscribers when pre-defined warning thresholds are exceeded. Note that only historical excavation prediction was available for this case study, and no practical early warnings can be issued. Thus, the presented warning models are empirical currently, and would be validated in future similar cut slopes.

7 Discussion

Like most landslide early warning systems implemented elsewhere, the implementation of warning models presented uses thresholds based on monitored landslide characteristics to issue warnings. Uncertainties of warning models exits inevitably because it is significantly difficult to define the accurate warning thresholds (Intrieri et al., 2012; Thiebes et al., 2014). According to the clear understanding of failure mechanism of this specific cut slope case, warning thresholds are confidently defined relying on a good correlation between toe excavation and actual surface displacement and the slope stability. In this study, through integrating the FEM slope stability analysis model into the warning model, the future safety status of the investigated cut slope can be reliably predicted based on the actual monitoring displacement and toe excavation, therefore, the warning models presented is deemed effective, even though no actual early warnings have yet been issued. However, this study still needs further investigation. Only one specific cut slope case investigated is insufficient. In order to refine the warning thresholds and reduce the frequency of false alarms, it is necessary to accumulate and analyze a larger number of similar cut slope cases.

As stated above, inappropriate toe excavation caused slope deformation, and the global excavation of the deformed slope would be effective for improving the stability of final excavated slope. However, it is important to consider that such global excavations of deformed slopes result in large volumes of materials, are expensive, are environmentally unfriendly, and may even unexpectedly induce secondary geological hazards under unfavorable geological and/or environmental conditions. Thus, appropriate excavation is essential for highway cut slopes, which should be further investigated. Pre-reinforced piles in front of such slopes have been proposed to temporarily or permanently restrain the potential slope deformation caused by toe excavation (Lirer, 2012; Xue et al., 2018). For this case, an additional excavation scheme was redesigned for FEM modelling (Figure 7). Scheme 1: Excas. 2, 3, and four are initially constructed, and Exca. 1 (toe excavation) is later constructed; Scheme 2: Only Exca. 1 is constructed after the installation of one row of

TABLE 2 Outline of the early warning system for excavation-induced soil landslide with a weak layer.

Early warning level		Attention	Caution	Vigilance	Alarm
Early warning parameter	Toe excavation $Ae(m^2)$	$Ae < 54.83$	$54.83 \leq Ae < 115.19$	$115.19 \leq Ae < 171.43$	$Ae \geq 171.43$
	Slope stability FoS	$FoS > 1.1$	$1.1 \geq FoS > 1.05$	$1.05 \geq FoS > 1.0$	$FoS \leq 1.0$
Deformation stage		Initial deformation	Constant deformation	Accelerative deformation	Failure
Landslide risk level		Low risk	Moderate risk	High risk	Very high risk
Counter-measures		Keep routine surface displacement monitoring	Keep routine surface and sub-surface displacement monitoring Implement field survey; warn the personnel	Keep close surface and/or sub-surface displacement monitoring Cease further toe excavation; Carry out emergency protection such as top excavation and toe surcharge	Keep closer surface displacement monitoring; Make the personnel and equipment evacuated promptly

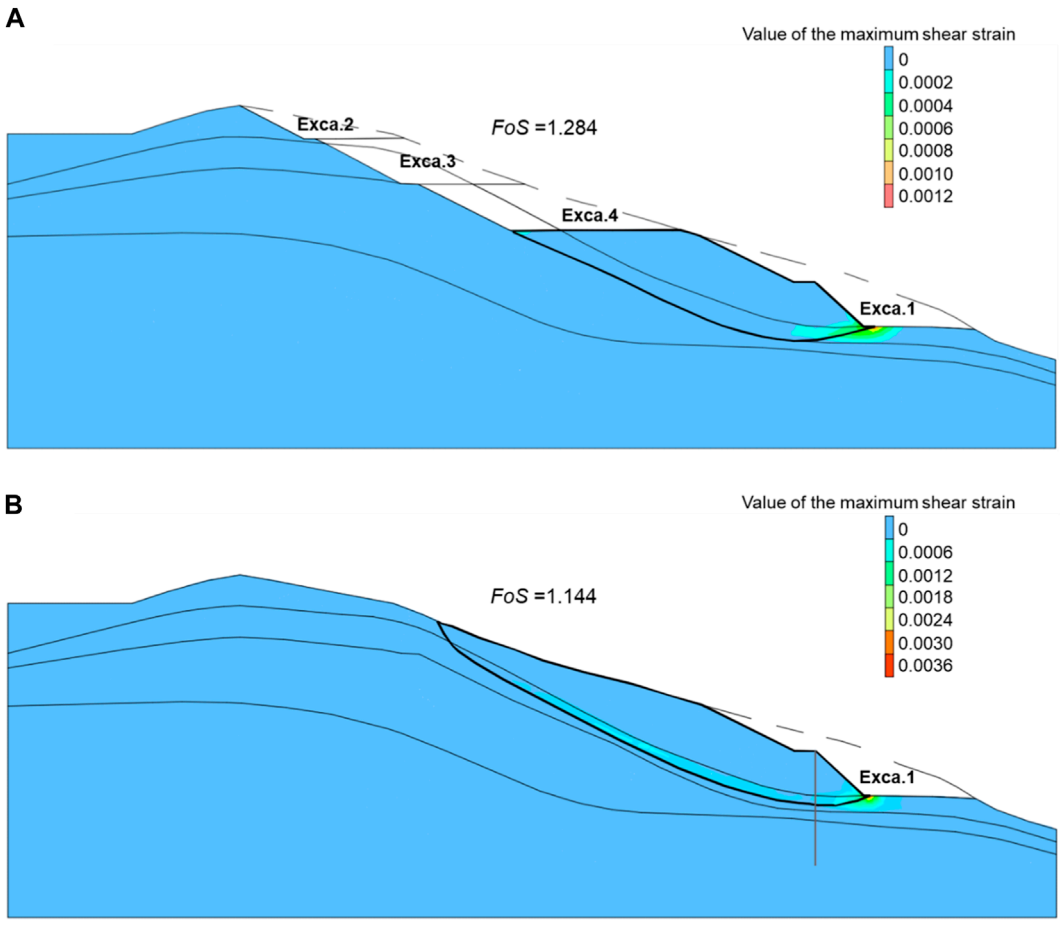

FIGURE 12
FEM results of the excavated slope stability for different schemes. **(A)**: Scheme 1: Excas. 2,3,4 are initially constructed, and Exca.1 is finally constructed, **(B)**: Scheme 2: Exca.1 is constructed after pre-reinforced pile installation.

pre-reinforced piles with a spacing of 5 m, a length of 20 m, and a cross-sectional area of 2 m × 3 m. The material properties are listed in Table 1.

After several series of FEM calculations, the maximum shear strain and the factor of safety FoS results for the excavated slope were obtained for the two schemes, as shown in Figure 12. Figures 8B, 12

show the position of the potential sliding surface can be directly influenced by the configuration of excavation; a well-developed sliding surface occurs for the original scheme (only toe excavation), whereas a poorly continuous sliding surface is formed for Scheme 1 and 2. Their respective slope stabilities are obviously distinct. Among them, Scheme 1, with the lowest maximum shear strain, corresponds to the largest factor of safety *FoS*, which is equal to 1.284. The factor of safety *FoS* for Scheme 2 using pre-reinforced piles to increase the slope stability is 1.144. According to the code for geological investigation of the landslide prevention, Scheme 1 satisfies the safety requirements. Accordingly, Scheme 1 is a preferable excavation scheme, as it ensures that the excavated slope is stable and is more cost-effective and environmental friendly than the global excavation scheme mentioned above.

8 Conclusion

A case study of a soil landslide experiencing obvious deformation during excavation for the construction of National Highway 351 was performed in this paper on the basis of detailed field reconnaissance and FEM simulations. The main conclusions are summarized as follows:

1. The occurrence of soil landslide are mainly attributed to the adoption of toe excavation and the presence of a silty clay layer. Detailed field reconnaissance of the slope prior to excavation is essential for minimizing the exposure of poor soil layer, thereby preventing potential landslides.
2. Toe excavation and surface displacement are adopted as warning indicators, and a four-level early warning system was established for further excavation-induced soil landslide. Thresholds of toe excavation and surface displacement for each warning level are defined depending on the resulting slope stability.
3. Top excavation prior to toe excavation, rather than global excavation of a soil landslide, is preferable for guaranteeing the required slope stability, because the global excavation could trigger new secondary landslides, especially when exposing unfavorable geological structures such as weak layers.

Data availability statement

The original contributions presented in the study are included in the article/Supplementary Material, further inquiries can be directed to the corresponding authors.

Author contributions

YW: Investigation, Writing–original draft, Writing–review and editing. DX: Conceptualization, Funding acquisition, Investigation, Methodology, Writing–original draft, Writing–review and editing. KC: Funding acquisition, Investigation, Writing–review and editing. CD: Investigation, Writing–review and editing. ZH: Investigation, Writing–review and editing. ZW: Investigation, Writing–review and editing. SZ: Conceptualization, Funding acquisition, Methodology, Software, Writing–review and editing, Writing–original draft.

Funding

The author(s) declare that financial support was received for the research, authorship, and/or publication of this article. This research is financially supported by Zhejiang Provincial Communication Department (No. 2023018), the Opening Fund of Key Laboratory of Geohazard Prevention of Hilly Mountains, Ministry of Natural Resources (Fujian Key Laboratory of Geohazard Prevention) (No. FJKLGH 2024K007), and the foundation of Key Laboratory of Soft Soils and Geoenvironmental Engineering (Zhejiang University), Ministry of Education (No. 2022P09).

Conflict of interest

The authors declare that the research was conducted in the absence of any commercial or financial relationships that could be construed as a potential conflict of interest.

Publisher's note

All claims expressed in this article are solely those of the authors and do not necessarily represent those of their affiliated organizations, or those of the publisher, the editors and the reviewers. Any product that may be evaluated in this article, or claim that may be made by its manufacturer, is not guaranteed or endorsed by the publisher.

References

Chen, Y., Zhao, L., Wang, Y., Jiang, Q., and Qi, D. (2019). Precipitation data and their uncertainty as input for rainfall-induced shallow landslide models. *Front. Earth Sci.* 13, 695–704. doi:10.1007/s11707-019-0791-7

Dick, G. J., Eberhardt, E., Cabrejo-Li´evano, A. G., Stead, D., and Rose, N. D. (2015). Development of an early-warning time-of-failure analysis methodology for open-pit mine slopes utilizing ground-based slope stability radar monitoring data. *Can. Geotechnical J.* 52, 515–529. doi:10.1139/cgj-2014-0028

Dikshit, A., Sarkar, R., Pradhan, B., Acharya, S., and Dorji, K. (2019). Estimating rainfall thresholds for landslide occurrence in the Bhutan Himalayas. *Water* 11, 1616. doi:10.3390/w11081616

Fan, X. M., Xu, Q., Alonso-Rodriguez, A., Subramanian, S. S., Li, W., Zheng, G., et al. (2019). Successive landsliding and damming of the Jinsha River in eastern Tibet, China: prime investigation, early warning, and emergency response. *Landslides* 16 (5), 1003–1020. doi:10.1007/s10346-019-01159-x

Fang, K., Miao, M. H., Tang, H. M., Dong, A., Jia, S., An, P., et al. (2022). Model test on deformation and failure behaviour of arching-type slope under excavation condition. *Eng. Geol.* 302, 106628. doi:10.1016/j.enggeo.2022.106628

Fang, K., Miao, M. H., Tang, H. M., Jia, S., Dong, A., An, P., et al. (2023). Insights into the deformation and failure characteristic of a slope due to excavation through

multi-field monitoring: a model test. *Acta Geotech.* 18, 1001–1024. doi:10.1007/s11440-022-01627-0

Gao, M. B., Zhang, H., Cui, S. H., Wu, Z., Liu, J., Feng, L., et al. (2022). Investigation on deformation mechanism and treatment effect of a scattered slope based on continuum–discontinuum element method and finite difference method. *Front. Earth Sci.* 10, 894923. doi:10.3389/feart.2022.894923

GEO-SLOPE International Ltd (2007) *GeoStudio tutorials*, 69. Calgary, Canada: Geo-Slope International Ltd.

Guzzetti, F., Gariano, S. L., Peruccacci, S., Brunetti, M. T., Marchesini, I., Rossi, M., et al. (2020). Geographical landslide early warning systems. *Earth-Science Rev.* 200, 102973. doi:10.1016/j.earscirev.2019.102973

Hiraoka, N., Kikkawa, N., Sasahara, K., Itoh, K., and Tamate, S. (2017). A full-scale model test for predicting collapse time using displacement of slope surface during slope cutting work. *Workshop World Landslide Forum*, 111–121. doi:10.1007/978-3-319-53487-9_12

Hungr, O., Leroueil, S., and Picarelli, L. (2014). The Varnes classification of landslide types, an update. *Landslides* 11 (2), 167–194. doi:10.1007/s10346-013-0436-y

Intrieri, E., Gigli, G., Mugnai, F., Fanti, R., and Casagli, N. (2012). Design and implementation of a landslide early warning system. *Eng. Geol.* 147, 124–136. doi:10.1016/j.enggeo.2012.07.017

Intrieri, E., Raspini, F., Fumagalli, A., Lu, P., Del Conte, S., Farina, P., et al. (2018). The Maoxian landslide as seen from space: detecting precursors of failure with Sentinel-1 data. *landslides* 15, 123–133. doi:10.1007/s10346-017-0915-7

Ju, N. P., Huang, J., He, C. Y., Van Asch, T., Huang, R., Fan, X., et al. (2020). Landslide early warning, case studies from Southwest China. *Eng. Geol.* 279, 105917. doi:10.1016/j.enggeo.2020.105917

Khanna, R., and Dubey, R. K. (2020). Comparative assessment of slope stability along road-cuts through rock slope classification systems in Kullu Himalayas, Himachal Pradesh, India. *Bull. Eng. Geol. Environ.* 12, 993–1017. doi:10.1007/s10064-020-02021-4

Lacasse, S., and Nadim, F. (2009). "Landslide risk assessment and mitigation strategy," in *Landslides-disaster Risk Reduction*. Editors K. Sassa, and P. Canuti (BerlinHeidelberg: Springer -Verlag), 31–61.

Li, J., Chen, S. X., and Yu, F. (2013). A method for searching potential failure surface of slope based on maximum shear strain increment. *Rock Soil Mech.* 34, 371–378. doi:10.16285/j.rsm.2013.s1.016

Li, M., Zhang, G., Zhang, J. M., and Lee, C. F. (2011). Centrifuge model tests on a cohesive soil slope under excavation conditions. *Soils Found.* 51 (5), 801–812. doi:10.3208/Sandf.51.801

Li, S. H., Wang, J. G., Liu, B. S., and Dong, D. P. (2007). Analysis of critical excavation depth for a jointed rock slope using a face-to-face discrete element method. *Rock Mech. Rock Eng.* 40 (4), 331–348. doi:10.1007/s00603-006-0084-9

Li, X. B., Cao, W. Z., Zhou, Z. L., and Zou, Y. (2014). Influence of stress path on excavation unloading response. *Tunn. Undergr. Space Technol.* 42 (42), 237–246. doi:10.1016/j.tust.2014.03.002

Lin, F., Wu, L. Z., Huang, R. Q., and Zhang, H. (2017). Formation and characteristics of the xiaoba landslide in fuquan, Guizhou, China. *Landslides* 15, 669–681. doi:10.1007/s10346-017-0897-5

Lirer, S. (2012). Landslide stabilizing piles: experimental evidences and numerical interpretation. *Eng. Geol.* 149, 70–77. doi:10.1016/j.enggeo.2012.08.002

Liu, S. H., Du, J., Yin, K. L., Zhou, C., Huang, C., Jiang, J., et al. (2024). Regional early warning model for rainfall induced landslide based on slope unit in Chongqing, China. *Eng. Geol.* 333, 107464. doi:10.1016/j.enggeo.2024.107464

Manconi, A., and Giordan, D. (2015). Landslide early warning based on failure forecast models: the example of the Mt. de La Saxe rockslide, northern Italy. *Nat. Hazards Earth Syst. Sci.* 15, 1639–1644. doi:10.5194/nhess-15-1639-2015

Medina-Cetina, Z., and Nadim, F. (2008). Stochastic design of an early warning system. *Georisk-Assessment Manag. Risk Eng. Syst. Geohazards* 2, 223–236. doi:10.1080/17499510802086777

Michoud, C., Bazin, S., Blikra, L. H., Derron, M. H., and Jaboyedoff, M. (2013). Experiences from site-specific landslide early warning systems. *Nat. Hazards Earth Syst. Sci.* 13, 2659–2673. doi:10.5194/nhess-13-2659-2013

Mirus, B., Morphew, M., and Smith, J. (2018). Developing hydro-meteorological thresholds for shallow landslide initiation and early warning. *Water* 10, 1274. doi:10.3390/w10091274

Mohammadi, S., and Taiebat, H. (2016). Finite element simulation of an excavation-triggered landslide using large deformation theory. *Eng. Geol.* 205, 62–72. doi:10.1016/j.enggeo.2016.02.012

Pecoraro, G., Calvello, M., and Piciullo, L. (2019). Monitoring strategies for local landslide early warning systems. *Landslides* 16, 213–231. doi:10.1007/s10346-018-1068-z

Pradhan, S. P., Vishal, V., and Singh, T. N. (2018). Finite element modelling of landslide prone slopes around Rudraprayag and Agastyamuni in Uttarakhand Himalayan terrain. *Nat. Hazards Earth Syst. Sci.* 94 (1), 181–200. doi:10.1007/s11069-018-3381-1

Stark, T. D., Arellano, W. D., Hillman, R. P., Hughes, R. M., Joyal, N., and Hillebrandt, D. (2005). Effect of toe excavation on a deep bedrock landslide. *J. Perform. Constr. Facil.* 19 (3), 244–255. doi:10.1061/(asce)0887-3828(2005)19:3(244)

Thiebes, B., Bell, R., Glade, T., Jäger, S., Mayer, J., Anderson, M., et al. (2014). Integration of a limit-equilibrium model into a landslide early warning system. *Landslides* 11, 859–875. doi:10.1007/s10346-013-0416-2

Wang, Z. Y., Gu, D. M., and Zhang, W. G. (2020). Influence of excavation schemes on slope stability: a DEM study. *J. Mt. Sci.* 17 (6), 1509–1522. doi:10.1007/s11629-019-5605-6

Won, J. Y., Cotton, B., and Porter, B. W. (2014). Deformation and shear strength behaviors of over consolidated clay from stress-path testing for a deep open cut excavation. *Geo-Congress*, 388–399. doi:10.1061/9780784413265.031

Wu, B. Q., and Wang, Y. (2020). Analysis on the influence of slope shape on the stability of highway soil slope. *Highw. Transp. Inn. Mong.* 176, 41–46. doi:10.19332/j.cnki.1005-0574.2020.02.010

Wu, L. L., He, K. Q., Guo, L., Zhang, J., Sun, L., and Jia, Y. (2022). Research on the excavation stability evaluation method of Chaqishan ancient landslide in China. *Eng. Fail. Anal.* 141, 106664. doi:10.1016/j.engfailanal.2022.106664

Xu, Q., Liu, H. X., Ran, J. X., Li, W., and Sun, X. (2016). Field monitoring of groundwater responses to heavy rainfalls and the early warning of the Kualiangzi landslide in Sichuan Basin, southwestern China. *Landslides* 13 (6), 1555–1570. doi:10.1007/s10346-016-0717-3

Xu, Q., Yuan, Y., Zeng, Y., and Hack, R. (2011). Some new pre-warning criteria for creep slope failure. *Sci. China-Technological Sci.* 54, 210–220. doi:10.1007/s11431-011-4640-5

Xu, Q., Zeng, Y., Qian, J. P., Wang, C. J., and He, C. J. (2009). Study on an improved tangential angle and the corresponding landslide pre-warning criteria. *Geol. Bull. China* 28 (4), 501–505. doi:10.1016/S1003-6326(09)60084-4

Xue, D. M., Li, T. B., Zhang, S., Ma, C., Gao, M., and Liu, J. (2018). Failure mechanism and stabilization of a basalt rock slide with weak layers. *Eng. Geol.* 233, 213–224. doi:10.1016/j.enggeo.2017.12.005

Zhang, G., Li, M., and Wang, L. P. (2014). Analysis of the effect of the loading path on the failure behaviour of slopes. *KSCE J. Civ. Eng.* 18 (7), 2080–2084. doi:10.1007/s12205-014-1461-7

Zhang, M., Nie, L., Xu, Y., and Dai, S. (2015). A thrust load-caused landslide triggered by excavation of the slope toe: a case study of the Chaancun Landslide in Dalian City, China. *Arabian J. Geosciences* 8 (9), 6555–6565. doi:10.1007/s12517-014-1710-6

Zhang, S. R., Jia, H., Wang, C., Wang, X., He, S., and Jiang, P. (2024). Deep-learning-based landslide early warning method for loose deposits slope coupled with groundwater and rainfall monitoring. *Comput. Geotechnics* 165, 105924. doi:10.1016/j.compgeo.2023.105924

Zhao, Y. Y., and Zhang, G. (2018) "Centrifuge model test on excavation-induced failure of soil slopes overlying bedrock," in *Proceedings of China-Europe Conference on Geotechnical Engineering* (Berlin, Germany: Springer International Publishing), 1570–1573. doi:10.1016/j.sandf.2020.06.009

Zhu, C., He, M. C., Murat, K., Cui, X., and Tao, Z. (2020). Investigating toppling failure mechanism of anti-dip layered slope due to excavation by physical modelling. *Rock Mech. Rock Eng.* 53, 5029–5050. doi:10.1007/s00603-020-02207-y

Zhu, L., He, S. M., Jian, J. H., Zhou, J., and Liu, B. (2021). Geological structure and failure mechanism of an excavation-induced rockslide on the Tibetan Plateau, China. *Bull. Eng. Geol. Environ.* 80, 1019–1033. doi:10.1007/s10064-020-02031-2